The International Journal of Advanced Manufacturing Technology (2023) 127:3385–3395
https://doi.org/10.1007/s00170-023-11718-1

ORIGINAL ARTICLE

A novel deflection control method for the asymmetric thin-walled component by optimizing the feed rate of the finishing process

Zhongxi Zhang[1] · Longhao Wang[1] · Shuaiqin Wang[1] · Dinghua Zhang[2] · Aituan Jiang[1]

Received: 31 October 2022 / Accepted: 3 June 2023 / Published online: 14 June 2023

Abstract

The complicated thin-walled components with asymmetric structure are extensively used in aerospace fields. The material of these parts is hard-to-machining (such as titanium alloy and superalloy) and the machining-induced residual stress (MIRS) is inevitable in each cutting process. The component is deformed easily after the MIRS is rebalanced, which has become one of the most important challenges for the manufacturing of these parts. To overcome this problem, a deflection control method for the asymmetric thin-walled component by optimizing the machining parameters of the finishing process is proposed, which is aimed at adjusting the distribution of MIRS and making the MIRS tends to be self-balanced. Firstly, the deflection of two typical thin-walled components, the thin-walled plate and the circular section plate, that caused by the symmetrically distributed MIRS is discussed in detail. The influence of the component structure on the deflection is revealed. Subsequently, the component is divided into different sub-regions and the optimization algorithm, includes the objective function and constraint, and is established to adjust the feed rate of each sub-region. To achieve the optimization, the mapping relationship between the deflection and the feed rate is established by combining the machining experiments and finite element method. And then, the method of adjusting the distribution of the MIRS based on the mapping relationship is presented, using which the component is divided into several sub-regions and the feed rate of each sub-region is optimized. Finally, two group machining experiments on the complex thin-walled blade are carried out. Experimental results illustrate that the proposed method can reduce the machining deflection obviously.

Keywords Thin-walled component · Asymmetric structure · Machining deflection · Residual stress · Feed rate optimization

1 Introduction

The complicated thin-walled parts with asymmetric structure, such as blade and casing, are the key components of aero-engine [1]. The higher geometric accuracy is needed to meet the performance of aero-engine, especially for the next-generation aero-engine [2]. However, the material of this component is usually hard-to-machining and the MIRS is generated inevitably due to the thermo-mechanical coupling of material removal process [3]. However, the existing machining process usually adopts the constant parameters, which leads to the MIRS is homogeneously distributed on the top surface of the material. However, the correspondence between the deflection and structure is ignored. The MIRS on the top surface of the component cannot be self-balanced. As a result, the component is deformed and scraped easily after the residual stress is redistributed, especially for finishing process [4].

During the machining of the thin-walled component, fixture plays a crucial link between the workpiece and machine tool [5]. It not only constrains the degrees of freedom and provides the supports, but also prevents the redistribution of residual stresses (i.e., internal stress and MIRS) in process [6]. The residual stresses rebalanced through deflection when the fixture is removed. Therefore, a series of studies on optimizing and adjusting the fixture are carried out. Xing [7] proposed a fully automated fixture layout optimization algorithm. On the base of the study, the fixture layout of the engine bracket was optimized by Ramachandran et al. [8]

✉ Zhongxi Zhang
zhongxizh@yzu.edu.cn

[1] College of Mechanical Engineering, Yangzhou University, Yangzhou 225127, Jiangsu, People's Republic of China

[2] Key Laboratory of High Performance Manufacturing for Aero Engine (Northwestern Polytechnical University), Ministry of Industry and Information Technology, Xi'an 710072, People's Republic of China

to reduce the deflection induced by drilling force. Gonzalo et al. [9] developed an active clamping unit by combining the locator and clamper, in which the casing is fixed without clamping stress. Wu et al. [10] built a new fixture-evaluation criteria for the adaptive CNC machining process of the near-net-shaped blade, and then, an adaptive fixture is developed by investigating the stiffness and the clamping sequence of the blade-fixture system. Hao et al. [11] divided the workpiece into fixed and floating region by a 6+X locating principle, and the floating units are used to support the floating region and adjusting the workpiece posture timely. It is noted that the fixture is adjusted after each machining process and the clamping stress is avoided in these methods. But the deflection will exceed the machining tolerance easily when the residual stress is large. On the contrary, Chatelain et al. [12] found that the deflection caused by external clamping force has a significant influence on stress distribution, but the value of the pre-deflection is set according to experience. Our team also presented an active control algorithm to accurately calculate the value of the in-process pre-deflection by combining the predicted and measured deflection [13]. The purpose of the methods is to balance the internal stress with MIRS and prevent the redistribution of residual stresses. Up to now, clamping the workpiece with a proper pre-stress before processing is an effective method for deflection control. However, the relatively complex calculation and operation of the fixture are not still completely avoided.

Another common implementation to improve the geometric accuracy of the thin-walled component is to first inspection the real geometry of the part and then adjusting the tool path. Liu et al. [14] presented a tool path adaptively adjusting method by inspection the interim machining states of the component. Xu et al. [15] presented a shape-adaptive milling method, which can adjust the nominal tool path to automatically adapt to the real geometry of the part. To improve the wall thickness error, Hao et al. [16] established a transplantation algorithm to generate the tool path that adaptive to the actual shape of the component, although there has been significant progress in eliminating the overcut and undercut. But the real geometry model should be reconstructed with the measured point cloud to redesign the tool path, which is still complex and time-consuming.

The redistribution of residual stresses is the main factor for machining deflection [17]. Therefore, researchers have tried themselves to improve the distribution of the residual through optimizing the machining process and parameters. In the method proposed by Cerutti and Mocellin [18], the machining sequence is optimized by considering the initial residual stress. Similarly, Hao et al. [19] established an autoregressive integrated moving average model to allocate the machining allowance dynamically to approach the minimum deflection. Li et. al [20] presented an optimization model to retain the appropriate finishing allowance, which is aimed at reducing the influence of initial residual stress on deflection. Alejandro et. al [21] established a neural network model to find the optimum parameters and machining locations to reduce the distortion of aircraft structures. Although the methods have achieved a good effect on deflection control, they are not suitable for the components that the material is hard-to-machining and the MIRS is dominant to the distortion [22]. Li et al. [23] decreased the deflection of an aviation thin-walled part by optimizing the axial cutting depth to control the profile and magnitude of the MIRS. Huang et al. [24] established the linear equations of MIRS increments based on the theory of linear inversion, which provides a new method to compute the desired machining parameters. Deng et al. [25] proposed a data-driven model to design the machining parameters according to the machining files with high quality. However, the structure of the most thin-walled parts is asymmetric and the deflection is closely related to the structure of the component. Therefore, the structure must be considered simultaneously when optimizing the machining parameters.

Targeting at the thin-walled component with asymmetrical structure, the research work presented a new deflection control method by considering the relationship between the deflection and structure. This method is dividing the surface of the component into several sub-region and optimizing the machining parameters of each sub-region. The remainder of the paper firstly analyzed the influence of the component structure on the MIRS induced deflection. In Section 3, a feed rate optimization algorithm, includes the objective function and constraints, is established. In Section 4, the mapping relationship between the deflection and the feed rate is established by combining the machining experiments and finite element simulation. The applicability and effectiveness of the proposed method are validated through machining a simplified compressor blade. The results of the experiment are discussed. Finally, the concluding remarks in Section 5.

2 The influence of the structure on machining deflection

To obtain the symmetrically distributed evenly MIRS, the symmetrical milling (see Fig. 1) is commonly used in the manufacturing of thin-walled blade part, especially for finishing milling. And then, the equivalent loads of MIRS on the top surface are symmetrical. However, the structure of the blade is asymmetrical and the equivalent loads of the MIRS cannot be balanced with each other. Therefore, the blade is easily deformed when the fixture is removed.

To prove the above point, the components are divided into two categories: exactly symmetrical to the neutral layer and asymmetric. Two simplified components (i.e., the flat plate,

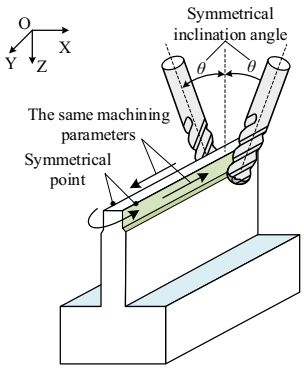

Fig. 1 The diagrammatic sketch of symmetrical machining

the circular section plate) are selected to reveal the influence of the component structure on machining deflection, in which the flat plate represents the simplified model of exactly symmetrical components and the circular section plate represents the simplified model of asymmetrical components. The principle of the finite element and the hexahedral element (see Fig. 2) are used to calculate the equivalent loads of MIRS and the deflection of component. The local coordinate system of each element is replaced by o_xyz and the global coordinate system of the component is replaced by $o\_\overline{xyz}$.

The MIRS on the top surface of the component can be expressed as:

$$\left\{\boldsymbol{\sigma}^{\mathbf{e}}\right\} = \left[\sigma_{11}^{u}\sigma_{22}^{u}\sigma_{11}^{l}\sigma_{22}^{l}\right]^{T} \tag{1}$$

where σ_{11}^{u} and σ_{22}^{u} are the MIRS on the upper surface of the component, σ_{11}^{l} and σ_{22}^{l} are lower surface.

The equivalent loads of the element nodes can be obtained by transplanting the MIRS to the element node. The equivalent load of each element is expressed as:

$$\left\{\mathbf{P}^{\mathbf{e}}\right\} = \left[P_{x1}P_{y1}P_{z1}P_{x2}P_{y2}P_{z2}\cdots P_{x8}P_{y8}P_{z8}\right]^{T} \tag{2}$$

where $\{\mathbf{P}^{\mathbf{e}}\}$ is the vector of equivalent load in o_xyz and $P_{xi}P_{yi}P_{zi}$ represent the equivalent load of the i^{th} node in the direction of o_x, o_y and o_z respectively, in which $i \in \{1, 2, \cdots, 8\}$.

Therefore, the equivalent loads of the MIRS can be obtained as:

$$P_{xi} = \sigma_{11}^{u} \bullet h_e l^e, P_{yi} = \sigma_{22}^{u} \bullet h_e l^e, P_{zi} = 0 \tag{3}$$

where h_e is the thickness of the MIRS-affected layer and the l^e is the size of the element.

Therefore, the relationship between the displacement and load of the element can be expressed as:

$$\mathbf{K}^{e} \bullet \mathbf{q}^{\mathbf{e}} = \mathbf{P}^{\mathbf{e}} \tag{4}$$

where $\mathbf{K}^{e}$ is the stiffness matrix of the element and $\mathbf{q}^{\mathbf{e}}$ is the displacement of element node and can be expressed as:

$$\left\{\mathbf{q}^{\mathbf{e}}\right\} = \left[u_1 v_1 w_1; u_2 v_2 w_2; \cdots; u_8 v_8 w_8\right]^{T} \tag{5}$$

where u_i, v_i, and w_i represent the displacement of the i^{th} node in the direction of o_x, o_y, and o_z respectively. The value of w_i can be obtained by combining Eqs. (3) and (4) (see Eq. (6)).

$$w_i = 0 \tag{6}$$

To calculate the displacement of each node in the global coordinate system, the coordinate transformation method is used and expressed as:

$$\overline{\mathbf{q}^{\mathbf{e}}} = \mathbf{T}^{e} \bullet \mathbf{q}^{\mathbf{e}} \tag{7}$$

where $\mathbf{T}^{e}$ is the coordinate transformation matrix and $\overline{\mathbf{q}^{\mathbf{e}}}$ represents the displacement of element node in the global coordinate system and can be expressed as:

$$\left\{\overline{\mathbf{q}^{\mathbf{e}}}\right\} = \left[\overline{u}_1 \overline{v}_1 \overline{w}_1; \overline{u}_2 \overline{v}_2 \overline{w}_2; \cdots; \overline{u}_8 \overline{v}_8 \overline{w}_8\right]^{T} \tag{8}$$

where $\overline{u}_i \overline{v}_i \overline{w}_i$ are the displacement of the i^{th} node in the direction of $o\_\overline{X}$, $o\_\overline{Y}$, and $o\_\overline{Z}$, in which $\overline{w}_i = 0$.

The deflection of the component can be obtained by superimposing the displacements of each node. And then, the deflection of the thin-walled plate and the circular section are analyzed by calculating the displacement of the element node.

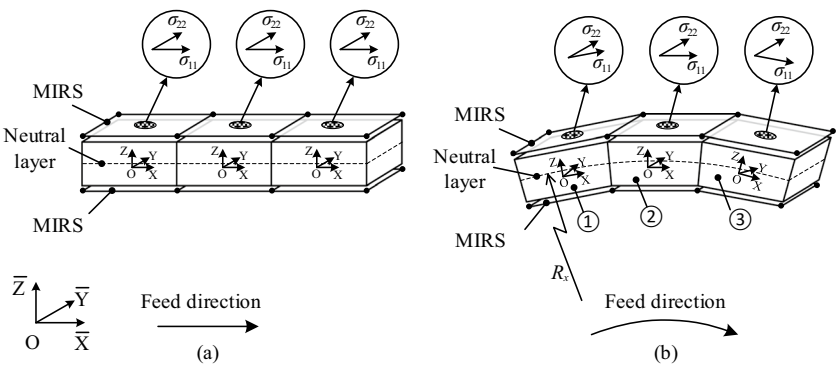

Fig. 2 The diagrammatic sketch of the finite element mesh: **a** flat plate; **b** circular section plate

(1) The exactly symmetrical component

The simplified model of exactly symmetrical component is flat plate, and the schematic of the equivalent loads of each element grid is shown in Fig. 3.

The element of the thin-walled plate is the regular hexahedron and the local coordinate system of the element is coincided with the global coordinate system. Therefore, the coordinate transformation matrix of the element is an identity matrix and expressed as:

$$\mathbf{T}_i^e = \begin{bmatrix} 1 & 0 & 0 \\ 0 & 1 & 0 \\ 0 & 0 & 1 \end{bmatrix} \tag{9}$$

The node displacement of each element in global coordinate system can be expressed as:

$$\overline{\mathbf{q}^e} = \mathbf{T}^e \bullet \mathbf{q}^e = \mathbf{q}^e \tag{10}$$

Equation (10) reflects that the displacements of each node in both global and local coordinate system is equal with each other and can be expressed as:

$$\begin{cases} \overline{u}_i = u_i; \\ \overline{v}_i = v_i; \\ \overline{w}_i = w_i = 0; \end{cases} \tag{11}$$

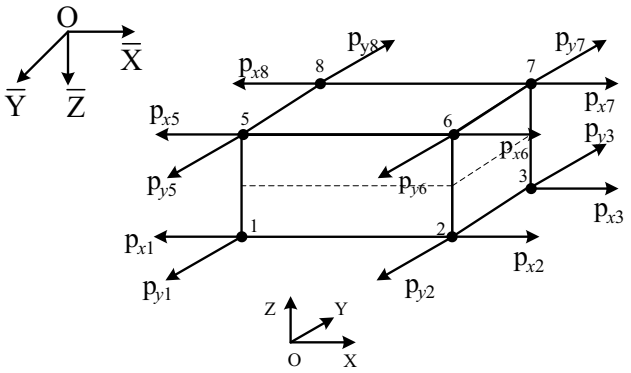

Fig. 3 The equivalent loads of flat plate

Therefore, the displacements of the node that symmetrical to the neutral layer are equal when the MIRS of the thin-walled plate is evenly distributed. The plate will extend tightly in the direction of o_$\overline{X}$ and o_$\overline{Y}$ and not deformed in the direction o_$\overline{z}$.

(2) The asymmetrical component

The simplified model of asymmetrical component is a circular section plate, and the schematic of the element equivalent loads is shown in Fig. 4. This time the elements are irregular hexahedron and the local coordinate system of the element cannot coincide with the global coordinate system of the component. To calculate the load and the displacement of the nodes, the element is replaced by ①, ②, and ③.

It assumed that the local coordinate system of is coinciding with the global coordinate. The angel between ① and ② in the direction o_x is replaced by θ. The angel between ② and ③ is α.

The coordinate transformation matrix of the element can be expressed as:

$$\mathbf{T}_i^{e_1} = \begin{bmatrix} \cos\theta & 0 & -\sin\theta \\ 0 & 1 & 0 \\ \sin\theta & 0 & \cos\theta \end{bmatrix} \tag{12}$$

where $\mathbf{T}_i^{e_1}$ is the coordinate transformation matrix of the element ①.

The coordinate transformation matrix of the element ② is:

$$\mathbf{T}_i^{e_2} = \begin{bmatrix} 1 & 0 & 0 \\ 0 & 1 & 0 \\ 0 & 0 & 1 \end{bmatrix} \tag{13}$$

where $\mathbf{T}_i^{e_2}$ is the coordinate transformation matrix of the element ②.

The coordinate transformation matrix of the element ③ is:

$$\mathbf{T}_i^{e_3} = \begin{bmatrix} \cos\alpha & 0 & \sin\alpha \\ 0 & 1 & 0 \\ -\sin\alpha & 0 & \cos\alpha \end{bmatrix} \tag{14}$$

Fig. 4 The equivalent loads of the circular section plate

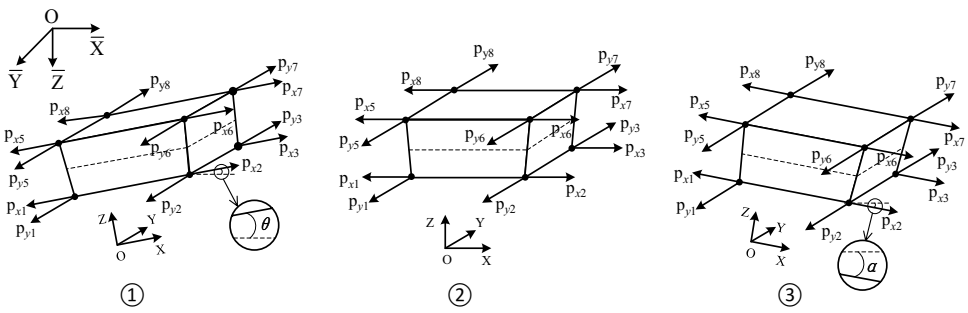

where $\mathbf{T}_i^{e_3}$ is the coordinate transformation matrix of the element ③.

Therefore, the node displacement of ① in global coordinate system can be expressed as:

$$\begin{cases} \overline{u}_i = \cos\theta\ u_i; \\ \overline{v}_i = v_i; \\ \overline{w}_i = \sin\theta\ u_i; \end{cases} \tag{15}$$

The node displacement of ② in global coordinate system can be expressed as:

$$\begin{cases} \overline{u}_i = u_i; \\ \overline{v}_i = v_i; \\ \overline{w}_i = w_i = 0; \end{cases} \tag{16}$$

The node displacement of ③ in global coordinate system can be expressed as:

$$\begin{cases} \overline{u}_i = \cos\theta u_i; \\ \overline{v}_i = v_i; \\ \overline{w}_i = -\sin\theta u_i; \end{cases} \tag{17}$$

Unlike flat plate, almost all the element nodes of the circular section plate are moved in the direction o_$\overline{z}$ (shown as Eqs. (15) and (17)), which means the circular section plate will be deformed in direction o_$\overline{z}$ with the evenly distributed MIRS.

Based on the above analysis, the equivalent loads of evenly distributed MIRS are self-balanced and the deflection is avoided when the structure of the component is exactly symmetrically to the neutral layer (such as flat plate). On the contrary, the equivalent loads are imbalanced and the component will be deformed when the structure is asymmetric to the neutral layer (such as circular section plate). Furthermore, the structure of the actual part is usually asymmetric, especially for the complicated thin-walled part of aero-engine. Therefore, the traditional method induced the evenly distributed MIRS on the top surface of the component. But the equivalent loads of the MIRS cannot be self-balanced and the deflection cannot be avoided. To eliminate the influence of the asymmetric of the component structure, a novel deflection control method is proposed to divide the surface of the component into several sub-region and optimize the machining parameters of each sub-region. So that the asymmetrically distributed MIRS can be induced on the surface of the component and the influence of the structural asymmetric is reduced.

3 Theoretical modeling

The MIRS is the coupling results of the mechanical and thermal loads of the cutting, in which the mechanical load results in the compressive stress and the thermal load leads to tensile stress. The profile of the MIRS will be different whether the mechanical or the thermal is changed. That means the MIRS is influenced by most of the machining parameters, in which the feed rate is the foremost [26]. Therefore, this study takes the feed rate as an example to change the distribution of the MIRS, which makes the MIRS of the final component tends to self-balancing and improves the machining accuracy. The method is realized by dividing the surface of the component into multi-sub-regions and optimizing the feed rate of each sub-region.

3.1 The objective function of the optimization

The processing will be complex and the machining stability is decreased if the machining parameters are changed continuously, especially for finishing milling. Therefore, the component is divided into multi-sub-regions by the feature of the geometric and the feed rate of each sub-region is constant (see Fig. 5). The MIRS of each sub-region can be expressed as a function of feed rate (see Eq. (18)):

$$h\left(f_z^j\right) = \left(\sigma_{11}, \sigma_{22}\right)^j \ (1 \le j \le \mathrm{n}) \tag{18}$$

where f_z^j and $\left(\sigma_{11}, \sigma_{22}\right)^j$ are the feed rate and the induced MIRS of the j^{th} sub-region, in which σ_{11} and σ_{22} are the components of the MIRS in the direction of feed and vertical of feed, and n is the total number of the sub-regions.

Finite element is the effective method to calculate the deflection of the component with complex structure [27]. MIRS of each sub-region is added as the loads of the finite element model. And then, the mapping relationship between the MIRS and deflection can be obtained (see Eq. (19)).

$$\mathbf{D} = F\left(\left(\sigma_{11}, \sigma_{22}\right)^1, \cdots, \left(\sigma_{11}, \sigma_{22}\right)^j, \cdots, \left(\sigma_{11}, \sigma_{22}\right)^n\right) \tag{19}$$

where $\mathbf{D}$ represents the deflection of the component.

The functional relationship between the feed rate and the deflection can be expressed as:

$$\mathbf{D} = F\left(h\left(f_z^j\right)\right) \ (1 \le j \le \mathrm{n}) \tag{20}$$

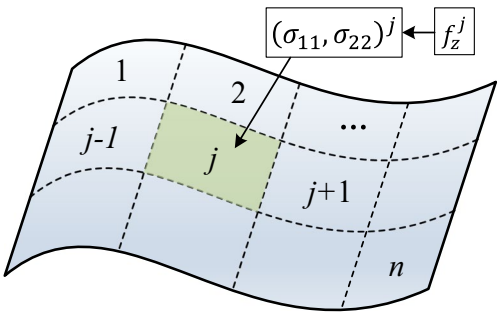

Fig. 5 The residual stress of the sub-region

The ultimate goal of the study is to minimize the deflection of the component. Therefore, the objective function can be simplified as:

$$\min : \mathbf{D} = F\left(h\left(f_z^j\right)\right) \tag{21}$$

3.2 The constraints

The optimized feed rate may exceed the stability region, which will lead to the instability of the processing and even damage the component or the machine. The unreasonable results can be avoided by adding the constraint.

The maximum allowable feed rate is limited by the performance of the machine tool, and the machining stability will be decreased whether the optimized feed rate reaches or exceeds the limit. Therefore, the optimized feed rate needs to be constrained by the maximum allowable value of the feed rate and the function of the constraint can be expressed as:

$$g_3\left(f_o\right) = f_o - \eta_3 f_{lim} \le 0 \tag{22}$$

where $g_3\left(f_o\right)$ is the constraint function of the feed rate, η_3 is the security coefficient, and f_{lim} is the maximum allowable of the feed rate.

3.3 The mapping relationship

The mapping relationship between the deflection and the feed rate is established by combining the machining experiments and simulation. Firstly, the thin-plate test is used to establish the functional relationship between the MIRS and the feed rate. And then, the mapping relationship between the deflection and the distribution of MIRS is obtained through FEM. The schematic diagram of the algorithm is shown in Fig. 6.

4 Case study

In this section, a typically asymmetrical component (the simplified compressor blade) is designed as the experimental part (see Fig. 7). The material of the blade is Ti-6Al-4V and the origin of the workpiece coordinate is set at the center of the blade tip. The thermal aging process is implemented to the blank part to minimize the influence of the initial stress.

The original coordinate system of the workpiece is the center of the blade tip. Four planar cross sections that parallel to YOZ are selected as the measuring cross sections (see Fig. 7), which are placed at X = 35 mm, 65 mm, 95 mm, and 125 mm, and denoted as A, B, C, and D respectively. Each section contains forty sampling points and the deflection of each point is measured by the on-machine measurement instrument (RENISHAW RMP600). The blade root is fixed throughout the machining, which is defined as the measurement datum. The blade tip is relaxed after machining, in which the MIRS is rebalanced and the blade surface is deformed. The deflection of the blade tip will be largest since it farthest from datum. Therefore, two points on the blade tip, denoted as OA and OB, are selected as the observation points to reflect the deflection of the blade tip, and the optimization is to minimize the deflection of the observation points.

4.1 The influence feed rate on MIRS

In this section, the thin-plate test is used to investigate the influence of feed rate on MIRS. The geometric size of the five plates is $80 \times 50 \times 1.5mm$. The machining parameters and equipment are shown in Table 1.

The deflection of the plates is measured by Alicona Infinitefocus G4. The MIRS of different feed rates is obtained by the algorithm presented in the article [28] and the results are shown in Fig. 8.

The least square method is used to fit the calculated value of the MIRS. The fitted functions are Eqs. (23) to (24) and the curves are shown in Fig. 9.

$$\sigma_{11} = -2113 f_z^3 + 4510 f_z^2 - 1510 f_z - 32.56 \tag{23}$$

$$\sigma_{22} = -1.33 * 10^4 f_z^3 + 1.13 * 10^4 f_z^2 - 2889 f_z - 75.08 \tag{24}$$

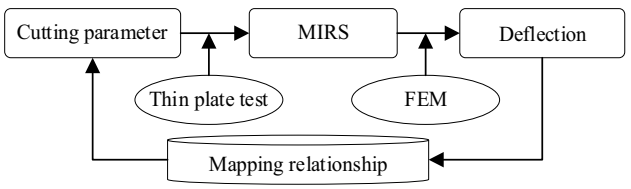

Fig. 6 The creation of the mapping relationship

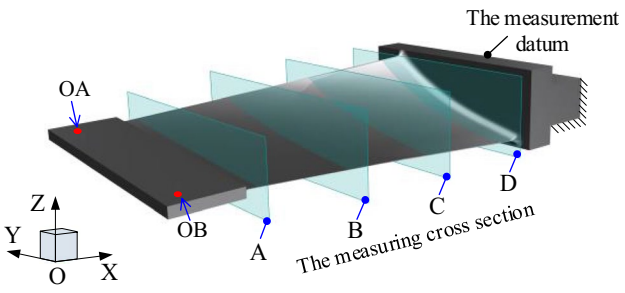

Fig. 7 The simplified model of the blade

Table 1 Machining parameters and equipment

Items	PA_1	PA_2	PA_3	PA_4	PA_5
Feed rate (mm/tooth)	0.1	0.15	0.2	0.25	0.3
Cutting speed (m/min)	50				
Axial cutting depth (mm)	0.5				
Radial cutting depth (mm)	0.5				
Lead angle	30°				
Machine	YH850Z				
Cutter material	Carbide				
Workpiece material	Ti-6Al-4V				
Cutter	12×R1×36×75 4F				
Cooling liquid	Water soluble coolant				
Measurement equipment	Alicona Infinitefocus G4				

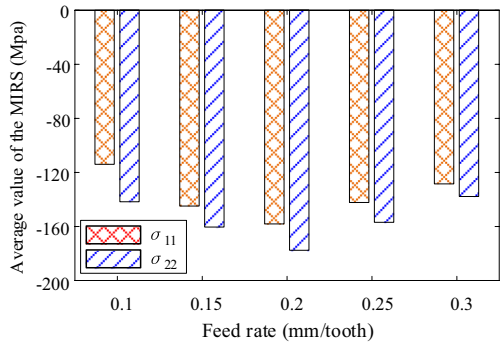

Fig. 8 The MIRS in different feed rate

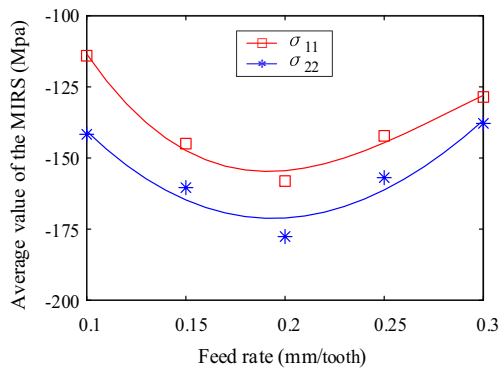

Fig. 9 The variation of the MIRS

4.2 The deflection response surface

To establish the deflection response surface, the blade surface is divided into two sub-regions (i.e., the concave surface and the convex surface). The feed rate of each sub-region (i.e., the concave surface and convex surface of the blade) is selected in sequence from the list in Fig. 10. After that, 25 kinds distributed residual stress are generated with

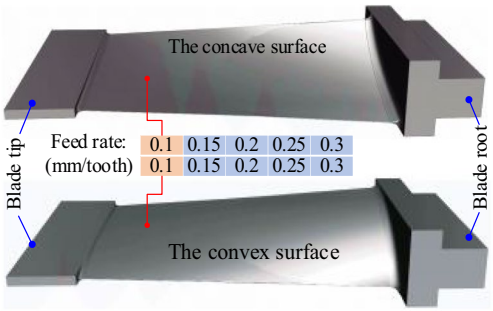

Fig. 10 The sub-regions of the blade and the parameter selection

the combination of feed rate in different sub-region. The deflection of the blade with different distributed residual stress is predicted by the finite element method. The loads of the model are the MIRS shown in Fig. 8. A 10-node quadratic tetrahedron (C3D10) type unit is used to mesh the part. The size of the mesh is 1 mm. The deflection of each observation point (OA and OB) is recorded.

The deflection of each observation point can be expressed as a five-dimensional matrix. The bi-cubic spline interpolation function (see Eq. (25)) is used to fit the simulated result.

$$r_{i,j}(u,w) = \begin{bmatrix} 1 & u & u^2 & u^3 \end{bmatrix} \mathbf{B} \mathbf{V} \mathbf{B}^{\mathbf{T}} \begin{bmatrix} 1 & w & w^2 & w^3 \end{bmatrix}^T \quad (0 < u, w < 1, i = 0, 1; j = 0, 1) \tag{25}$$

where $r_{i,j}(u,w)$ is the fitted result of the deflection, u and w are the parameters of the surface, $\mathbf{V}$ is the deflection matrix of the observation point, and $\mathbf{B}$ is the coefficient matrix which is expressed as:

$$\mathbf{B} = \frac{1}{6}\begin{bmatrix} 1 & 4 & 1 & 0 \\ -3 & 0 & 3 & 0 \\ 3 & -6 & 3 & 0 \\ -1 & 3 & -3 & 1 \end{bmatrix} \tag{26}$$

The deflection response surface of the observation points (i.e., OA and OB) can be obtained (see Fig. 11 and Fig. 12).

4.3 Feed rate optimization

According to the above analysis, the deflection of the component is concentrated on the observation points. Therefore, an evaluation function (see Eq. (27)) is established to optimize the feed rate of each sub-region, which is aimed at minimizing deflection of the observation points simultaneously. The deflection of the component reaches the minimum only when the value of the evaluation function is minimized.

$$F_e\left(f_z^1, f_z^2\right) = {D_{OA}}^2 + {D_{OB}}^2 \tag{27}$$

where $F_e\left(f_z^1, f_z^2\right)$ is the evaluation function of the optimization objective and D_{OA} and D_{OB} represent the deflection of the observation points respectively.

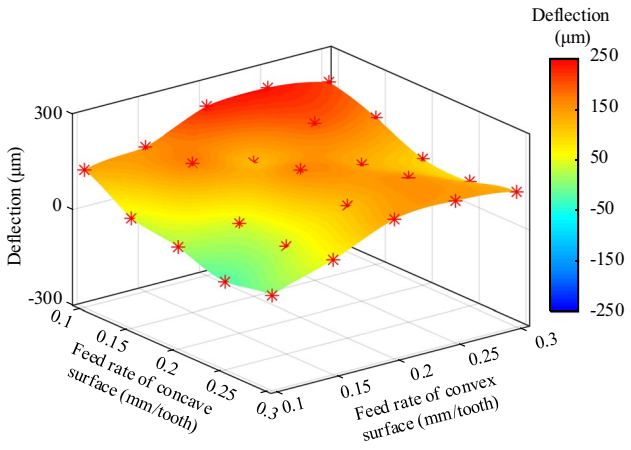

Fig. 11 The deformation response surface of OA

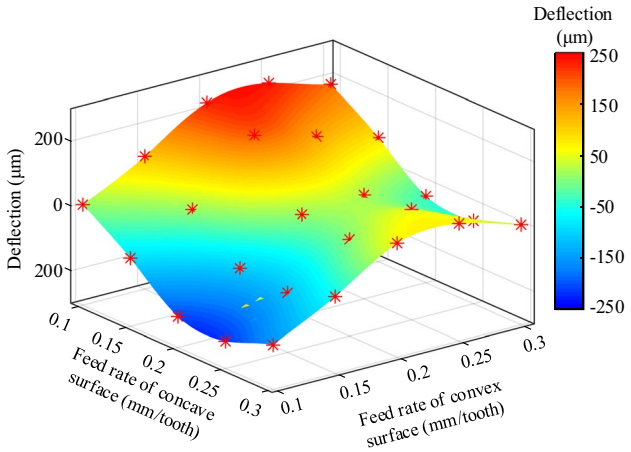

Fig. 12 The deflection response surface of OB

Ultimately, the optimized feed rate can be obtained by substituting the deflection of observation points (shown in Fig. 11 and Fig. 12) into Eq. (27) and the results are:

$$f_z^1 = 0.23, f_z^2 = 0.1 \tag{28}$$

where f_z^1 and f_z^2 are the optimized feed rate of concave and convex surface of the blade respectively.

By now, the deflection of the observation points are:

$$D_{OA} = 63.3\mu m, D_{OB} = -40.6\mu m \tag{29}$$

4.4 Cutting experiment and analysis

In this section, two group actual machining experiments are carried out to verify the effectiveness of the optimized results. Two blades are processed with different machining schemes, in which the first blade is processed with the constant feed rate and the second blade is processed with the optimized feed rate. The blades are processed with same cutter and the new cutter is used in each machining process to minimize the influence of tool wear. The feed rates of the blades are shown in Table 2. The remaining parameters and the equipment are same with the thin-plate test (see Table 1).

Table 2 The feed rate of the blade

Items	The first blade	The second blade
f_z^1(mm/tooth)	0.15	0.23
f_z^2(mm/tooth)	0.15	0.1

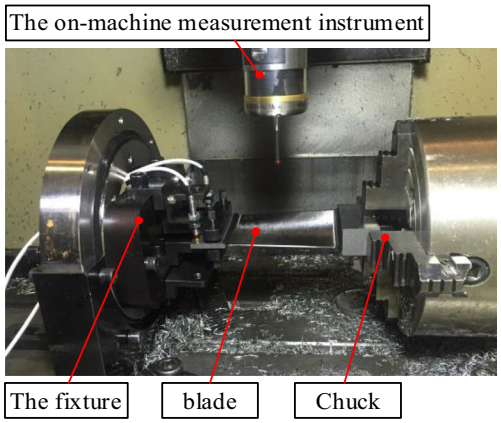

Fig. 13 The machining process of the blade

The machining process of the blade is shown in Fig. 13. The blade root is clamped by the chuck of the machine. The blade tip is fixed by the special fixture, which is introduced in the previously published article. The on-machine measurement instrument RENISHAW RMP600 is used to measure the coordinate of the sampling points and calculate the deflection of the blade.

The least square method is used to fit the measured results and the nephograms of the deflection are shown in Fig. 14. The dash lines in the figures represent the measuring cross sections of the blade. The results reflect that the deflection of the second blade is reduced significantly than the first blade.

The blade root remains fixed as the datum throughout the measurement process. The first measuring cross section (i.e., A) is far away from measurement datum, and the last measuring cross section (i.e., D) is close to the measurement datum. The measurement results and the fitted line of the blades are shown in Fig. 15. The abscissa of the figures represents the Y-axis coordinate of the sample points, and the ordinate is the deflection, to which the following discussion is offered.

Figure 15a represents the distortion of the first measuring cross section that is close to the blade tip, which is far

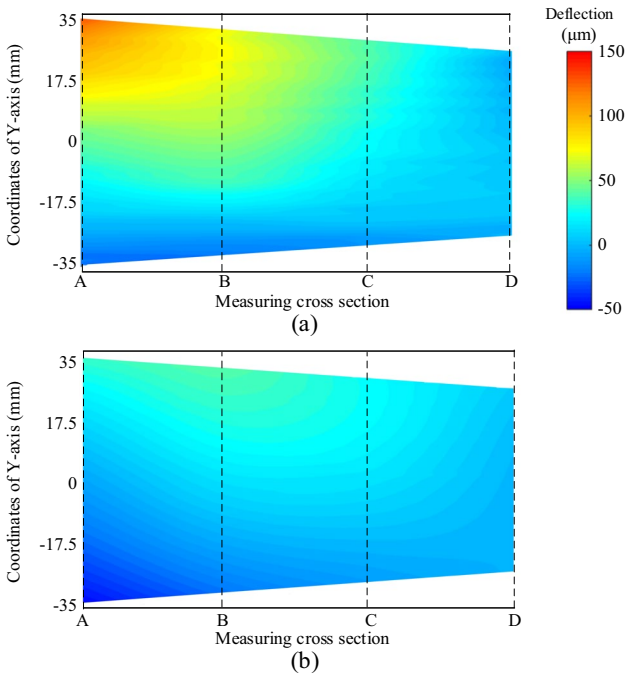

Fig. 14 The deflection of the blade: **a** before optimization. **b** After optimization

from the datum and keep free throughout measurement. Therefore, the measured value at this position is the largest. On the contrary, Fig. 15d represents the distortion of the last measuring cross section that is close to the blade root. The blade root has a greater rigidity due to the large thickness. Therefore, the blade is not easy to deformed in this measuring cross section.

For the first blade, the convex surface and the concave surface are processed with the constant feed rate (i.e., $f_z^1 = f_z^1 = 0.15$ mm/tooth). After machining, the MIRS on the top layer of the blade is distributed homogeneously. However, the structure of the blade is asymmetric and the equivalent loads of the MIRS in convex and concave surface cannot be balanced each other, which results in a larger deflection.

For comparison, the second blade is processed with the optimized parameter, in which the feed rates of the convex surface and the concave surface are different (i.e., $f_z^1 = 0.23$, $f_z^1 = 0.15$ mm/tooth). After machining, the MIRS of the convex surface is different from the concave surface. The equivalent loads of MIRS are asymmetric and the effect is balanced with the asymmetric structure, as clearly validated by the markedly reduced deflection shown in Fig. 15.

For a better view of comparison, the deflection of the blades is further quantitatively analyzed in Fig. 16, while the histograms in the figure indicate the improvement of deflection at each measuring cross section. After the optimization, the maximum deflection of the blade reduced by 93 μm, and the reduction rate is 43.87%. The reduction values of each measuring cross section are also shown in the figure.

Fig. 15 The measured results of each measuring cross section: **a** cross section A; **b** cross section B; **c** cross section A; **d** cross section D

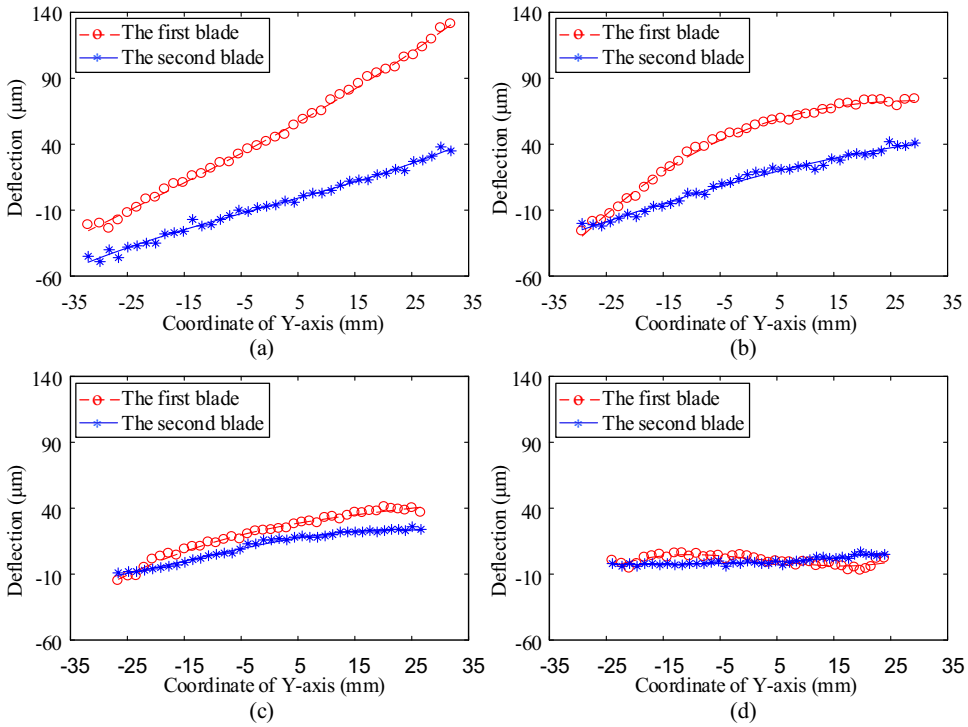

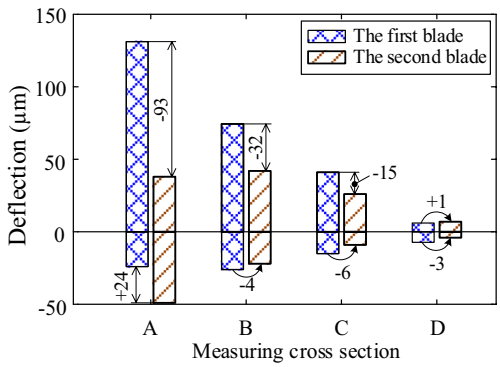

Fig. 16 The comparison of the maximum deflection of each measuring section

5 Conclusion

In this paper, a novel feed rate optimization method is presented to reduce the MIRS induced deflection of the thin-walled component with asymmetric structure. The main idea is to optimize the feed rate of the component, which makes the MIRS on the top layer of the component asymmetrically distributed. And then, the equivalent loads of MIRS are self-balanced and the induced deflection is reduced significantly. The main contributions of this paper can be concluded as following:

(1) The MIRS induced deflection of thin-walled plate and circular section plate are analyzed by calculating the displacement of the element nodes. The influence of structure on the deflection of the component is revealed.
(2) The mapping relationship between the deflection and the feed rate is established by combining the thin-plate test and the FEM, which is the basis for establishing the mathematical model and optimizing the feed rate.
(3) The validation demonstrates that the proposed feed rate optimization method is able to significantly reduce the deflection of the simplified blade. The reduction rate of the maximum deflection is 43.87%.

This study is first attempted to control the MIRS induced deflection by optimize the machining parameters and the effectiveness of the method is validated by machining experiments. However, other parameters that have obvious effect on MIRS are constant in this study and the deflection of the final component is not completely eliminated. Further research with a large amount of cutting experiments will be carried out to establish the mapping relationship between MIRS and machining parameters to optimize the additional parameters in the future.

Author contribution Zhongxi Zhang designed the framework of the paper and wrote the manuscript. Longhao Wang and Shuaiqin Wang carried out the experiments and provided data analysis. Dinghua Zhang and Zhongxi Zhang contributed to the main idea of the paper. Aituan Jiang polished the manuscript.

Funding This study was co-supported by the Research Fund of the National Natural Science Foundation of China (Grant No. 52205501), the Key Laboratory of High Performance Manufacturing for Aero Engine (Northwestern Polytechnical University), Ministry of Industry and Information Technology (Grant No. HPM-2021-04), and the National Natural Science Foundation of China (Grant No. 91860206).

Declarations

Ethical approval Not applicable.

Consent to participate Not applicable.

Consent for publication Not applicable.

Conflict of interest The authors declare no competing interests

References

1. Mali RA, Gupta TVK, Ramkumar J (2021) A comprehensive review of free-form surface milling– advances over a decade. J Manuf Process 62:132–167. https://doi.org/10.1016/j.jmapro.2020.12.014
2. Luo M, Luo H, Axinte D et al (2018) A wireless instrumented milling cutter system with embedded PVDF sensors. Mech Syst Signal Process 110:556–568. https://doi.org/10.1016/j.ymssp.2018.03.040
3. Guo J, Fu H, Pan B, Kang R (2021) Recent progress of residual stress measurement methods: a review. Chinese J Aeronaut 34:54–78. https://doi.org/10.1016/j.cja.2019.10.010
4. Wang Z, Sun J, Liu L, et al (2019) An analytical model to predict the machining deformation of frame parts caused by residual stress. J Mater Process Technol 274:. https://doi.org/10.1016/j.jmatprotec.2019.116282
5. Gameros A, Lowth S, Axinte D et al (2017) State-of-the-art in fixture systems for the manufacture and assembly of rigid components: a review. Int J Mach Tools Manuf 123:1–21
6. Li Y, Liu C, Hao X et al (2015) Responsive fixture design using dynamic product inspection and monitoring technologies for the precision machining of large-scale aerospace parts. CIRP Ann Manuf Technol 64:173–176. https://doi.org/10.1016/j.cirp.2015.04.025
7. Xing YF (2017) Fixture layout design of sheet metal parts based on global optimization algorithms. J Manuf Sci Eng Trans ASME 139:1–10. https://doi.org/10.1115/1.4037106
8. Ramachandran T, Surendarnath S, Dharmalingam R (2020) Engine-bracket drilling fixture layout optimization for minimizing the workpiece deformation. Eng Comp (Swansea, Wales) 38:1978–2002. https://doi.org/10.1108/EC-04-2020-0194
9. Gonzalo O, Seara JM, Guruceta E et al (2017) A method to minimize the workpiece deformation using a concept of intelligent fixture. Robot Comput Integr Manuf 48:209–218. https://doi.org/10.1016/j.rcim.2017.04.005
10. Wu D, Wang H, Peng J et al (2020) Machining fixture for adaptive CNC machining process of near-net-shaped jet engine blade. Chinese J Aeronautics 33:1311–1328

11. Hao X, Li Y, Chen G, Liu C (2018) 6+X locating principle based on dynamic mass centers of structural parts machined by responsive fixtures. Int J Mach Tools Manuf 125:112–122. https://doi.org/10.1016/j.ijmachtools.2017.11.006
12. Chatelain JF, Lalonde JF, Tahan AS (2012) Effect of residual stresses embedded within workpieces on the distortion of parts after machining. Int J Mech 6:43–51
13. Zhang Z, Luo M, Tang K, Zhang D (2020) A new in-processes active control method for reducing the residual stresses induced deformation of thin-walled parts. J Manuf Process 59:316–325
14. Liu C, Li Y, Hao X (2017) An adaptive machining approach based on in-process inspection of interim machining states for large-scaled and thin-walled complex parts. Int J Adv Manuf Technol 90:3119–3128. https://doi.org/10.1007/s00170-016-9647-4
15. Xu J, Xu L, Li Y, Sun Y (2020) Shape-adaptive CNC milling for complex contours on deformed thin-walled revolution surface parts. J Manuf Process 59:760–771. https://doi.org/10.1016/j.jmapro.2020.10.001
16. Hao X, Li Y, Deng T et al (2019) Tool path transplantation method for adaptive machining of large-sized and thin-walled free form surface parts based on error distribution. Robot Comput Integr Manuf 56:222–232. https://doi.org/10.1016/j.rcim.2018.10.007
17. Mocellin K, Cerutti X (2016) Numerical prediction of distortions during machining of large aluminium aeronautical parts. Mater Sci Eng Technol 47:699–709. https://doi.org/10.1002/mawe.201600603
18. Cerutti X, Mocellin K (2016) Influence of the machining sequence on the residual stress redistribution and machining quality: analysis and improvement using numerical simulations. Int J Adv Manuf Technol 83:489–503. https://doi.org/10.1007/s00170-015-7521-4
19. Hao X, Li Y, Huang C et al (2020) An allowance allocation method based on dynamic approximation via online inspection data for deformation control of structural parts. Chinese J Aeronautics 33:3495–3508. https://doi.org/10.1016/j.cja.2020.03.038
20. Li X, Li L, Yang Y et al (2020) Machining deformation of single-sided component based on finishing allowance optimization. Chinese J Aeronautics 33:2434–2444. https://doi.org/10.1016/j.cja.2019.09.015
21. Rodríguez-Sánchez AE, Ledesma-Orozco E, Ledesma S (2020) Part distortion optimization of aluminum-based aircraft structures using finite element modeling and artificial neural networks. CIRP J Manuf Sci Technol 31:595–606. https://doi.org/10.1016/j.cirpj.2020.08.011
22. Akhtar W, Lazoglu I, Liang SY (2022) Prediction and control of residual stress-based distortions in the machining of aerospace parts: a review. J Manuf Process 76:106–122. https://doi.org/10.1016/j.jmapro.2022.02.005
23. Li B, Jiang X, Yang J, Liang SY (2015) Effects of depth of cut on the redistribution of residual stress and distortion during the milling of thin-walled part. J Mater Process Technol 216:223–233. https://doi.org/10.1016/j.jmatprotec.2014.09.016
24. Huang K, Yang W, Ye X (2018) Adjustment of machining-induced residual stress based on parameter inversion. Int J Mech Sci 135:43–52
25. Deng T, Li Y, Liu X et al (2021) A data-driven parameter planning method for structural parts NC machining. Robot Comput Integr Manuf 68:102080. https://doi.org/10.1016/j.rcim.2020.102080
26. Wan M, Ye XY, Yang Y, Zhang WH (2017) Theoretical prediction of machining-induced residual stresses in three-dimensional oblique milling processes. Int J Mech Sci 133:426–437. https://doi.org/10.1016/j.ijmecsci.2017.09.005
27. Korkmaz ME, Gupta MK (2023) A state of the art on simulation and modelling methods in machining: future prospects and challenges. Arch Computat Methods Eng 30:161–189. https://doi.org/10.1007/s11831-022-09794-9
28. Zhang Z, Zhang Z, Zhang D, Luo M (2020) Milling distortion prediction for thin-walled component based on the average MIRS in specimen machining. Int J Adv Manuf Technol 111:3379–3392. https://doi.org/10.1007/s00170-020-06281-y